J. Appl. Comput. Mech., 4(1) (2018) 1-15
DOI: 10.22055/JACM.2017.21820.1117

ISSN: 2383-4536
jacm.scu.ac.ir

Journal of
Applied and Computational Mechanics

Research Article

Buckling Analysis of a Micro Composite Plate with Nano Coating Based on the Modified Couple Stress Theory

Mohammad Malikan[1]

[1] Department of Mechanical Engineering, Faculty of Engineering, Islamic Azad University, Mashhad, Iran

Received April 20 2017; Revised May 16 2017; Accepted for publication May 17 2017.
Corresponding author: Mohammad Malikan, mohammad.malikan@yahoo.com

Abstract. The present study investigates the buckling of a thick sandwich plate under the biaxial non-uniform compression using the modified couple stress theory with various boundary conditions. For this purpose, the top and bottom faces are orthotropic graphene sheets and for the central core the isotropic soft materials are investigated. The simplified first order shear deformation theory (S-FSDT) is employed and the governing differential equations are obtained using the Hamilton's principle by considering the Von-Karman's nonlinear strains. An analytical approach is applied to obtain exact results with different boundary conditions. Due to the fact that there is no research on the stability of micro/nano sandwich plates based on S-FSDT including the couple stress effect, the obtained results are compared with the FSDT studies which use the Eringen nonlocal elasticity.

Keywords: Thick sandwich plate; Modified couple stress theory; S-FSDT.

1. Introduction

The graphene structures represent 2D plane sheets of covalently bonded carbon atoms that form ideal hexagonal crystal lattices with the low weight and the high strength. The graphene specimens typically exist as either monolayers attached to substrates made of another material [1]. Due to the ultrahigh strength of the graphene, its inclusions are effectively used in the enhancement of both strength and fracture toughness in composite materials [2]. For instance, in order to improve the fracture toughness of ceramic materials, several research groups fabricated nano composites consisting of ceramic matrixes and inclusions in the form of graphene platelets [2, 3]. Moreover, inclusions in the form of graphene sheets provided enhancement of mechanical characteristics in the polymer-based nano composites [4]. For instance, partially oxygenated graphene sheets were dispersed in the polymer matrix, and mechanical characteristics of resultant nano composites with various graphene contents were examined [5].

The micro/nano composite material is a type of the sandwich formed from two thin skins of graphene bonded to a polymer or soft metal core in a continuous process under controlled pressure, heat, and tension. The most commonly used sandwich theory is linear and is an extension of first order beam theory. The linear local buckling sandwich theory is importance for the design and analysis of sandwich plates which are used in the building construction, the vehicle construction, the airplane construction and the refrigeration engineering [6].

Polymers are used in a broad range of applications especially due to their light weight, low cost, flexibility and easy processing. However, compared to ceramics and metals, polymers have weaknesses in terms of low stiffness and strength which limit their use. Therefore, adding rigid fillers in the nanometer size to reinforce the polymer matrices leads to a new class of materials [7].

Published Online: October 27 2017

Due to difficulties encountered in the experimental characterization of nano material, the theoretical approach is employed. Heretofore, the micro/nano sandwich plate with graphene coating that oriented theoretically by using new methods (to the best of the author's knowledge) is not taken into consideration. On the contrary, regarding the mechanical behavior of nano sheets, extensive and theoretical studies in the last several years have been conducted. Malekzadeh et al. [8] considered the small scale effect on the thermal buckling of orthotropic arbitrary straight-sided quadrilateral nano
plates embedded in an elastic medium via the classical plate theory. Zenkour and Sobhy [9] analyzed the thermal buckling of a rectangular nano graphene sheet based on the Winkler-Pasternak foundation. The sine function and the sinusoidal plate theory were used to derive the equations. Murmu et al. [10] conducted the buckling analysis of the bi-layer nano graphene in the nonlocal theory under the biaxial compression via the analytical solution using the classical plate theory with linear strains. It also demonstrated that the nonlocal critical load was always less than the local critical load. Wang et al. [11] investigated the thermal buckling of the nano scale plate via the classical and Mindlin plate theory by using simply supported boundary condition. Malekzadeh and Alibeygi [12] analyzed the thermal buckling of an orthotropic single layer graphene sheet using the nonlinear elastic foundation. The classical theory and the differential quadrature method were used together with the Winkler elastic foundation which was modeled with the nonlinear spring. This method serves as a bench mark for future research. Mohammadi et al. [13] studied the shear buckling of an orthotropic rectangular single layer nanoplate in the thermal environment by the classical plate theory. They showed that the difference between the shear buckling load calculated by isotropic and orthotropic plates decreased by increasing the nonlocal parameter. Radic et al. [14] published a study on the mechanical buckling of the multi-layer rectangular graphene sheet based on an elastic foundation and found that the nonlocal effect had great influence on higher buckling modes. The exact solution for vibrations and the biaxial buckling of multi-layer graphene sheet based on the Winkler elastic foundation were investigated by Murmu et al. [15]. The presented equations utilized the classical plate theory and proved that the critical temperature and natural frequencies were further affected by reducing the Winkler coefficient in high modes. Anjomshoa et al. [16] derived mechanical buckling equations of the multi-layer rectangular graphene sheet placed on an elastic foundation using the classical plate theory and the finite element numerical method. Radebe and Adali [17] studied the buckling of rectangular nanoplates with uncertain orthotropic material properties using the non-local theory. They considered the nanoplate as a non-local plate to take the small-size effects into account along with the small-scale parameter also to be taken as uncertain. They studied the effect of the small scale on natural frequencies. A new analytical solution for the buckling and vibration analysis of functionally graded sandwich beams using a quasi-3D shear deformation theory was presented by Nguyen et al. [18]. Golmakani and Rezatalab [19] conducted a study on the biaxial buckling of a single layer graphene plate by considering the elastic foundation and the non-uniform mechanical load. The results showed that by neglecting the elastic foundation, when the small scale effects were reduced, the critical load also decreased. Jamali et al. [20] presented the uniaxial buckling analysis comparison of the nanoplate and the nanocomposite plate with the central square cut out by using the domain decomposition method. They showed that the existence of a hole in the plate causes defect in the system and weakens the buckling behavior. Radic and Jeremic [21] studied the thermal buckling of double-layered graphene sheets embedded in an elastic medium with various boundary conditions using a nonlocal new first-order shear deformation theory. Their results showed that in nonlinear distributions of temperature all over the thickness of the plate, a higher value of critical buckling temperatures is obtained for lower values of the aspect ratio. The dynamic buckling of embedded laminated nanocomposite plates based on the sinusoidal shear deformation theory was studied by Zarei et al. [22]. Malikan et al. [23] published the buckling of the double-layered nanoplate under shear and thermal loads based on the elastic matrix using the differential quadrature method. They showed that the effect of the type of shear loading on the nonlocal results was more significant than local results. Moreover, while in the thermal buckling analysis the most important results implied whether the boundary conditions had more flexibility, by increasing the dimension's ratio, the results of critical temperature were tightly close together in the nonlocal and local analysis.

The main aim of this study is to give a brief overview of new theoretical considerations on nanocomposite sheets under the biaxial buckling. Regarding FSDT, we could not get the right value for the shear correction factor to consider the shear stress distribution in the thickness direction. Therefore, the simplified first order shear deformation theory (S-FSDT) that provides a welcome alternative to solve this problem is investigated. In the following section, the nonlinear strain of Von-Karman is considered. In addition, in order to study the length scale, the modified couple stress effect is employed because there is a difficulty in the Eringen nonlocal elasticity to consider nano materials behavior. The Eringen nonlocal elasticity is applied on the nonlocal stress resultants to derive governing equations because the nonlocal parameter is variable. Moreover, the exact solution is used to solve the stability equations. Finally, the effects of different parameters including changes in the core thickness, the aspect ratio and boundary effects of edges in various conditions under the nonuniform in-plane loads are demonstrated.

2. Formulation

A rectangular sandwich panel is considered with the thickness t_1 for faces, t_2 for the core ($h=2t_1+t_2$), the length L_x, and the width L_y as shown in Fig.1. Of the many shear deformable plate theories proposed over the years, the FSDT is fundamentally simpler to adopt for modelling the shear deformation behavior of plates. FSDT, is widely used even today because of its simplicity. Nowadays, it is well-known that in the plate analysis, shear deformation effects are important not only for thick plates but even for thin plates [24]. As the classical plate theory (CPT) does not take into account shear effects, many theories got evolved to address the deficiency. According to the FSDT, the following displacement field can be expressed as:

$$U\left(x,y,z\right)=u\left(x,y\right)+z\,\varphi\left(x,y\right) \tag{1a}$$

$$V(x,y,z) = v(x,y) + z\psi(x,y) \tag{1b}$$

$$W(x,y,z) = w(x,y) \tag{1c}$$

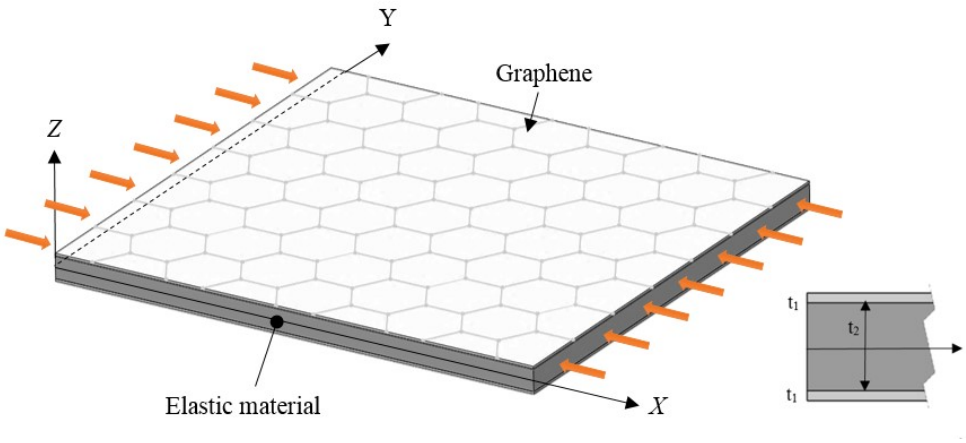

Fig. 1. Schematic diagram of the sandwich plate

Where u, v and w are the displacement components along x, y and z directions, respectively. Moreover, φ and ψ are the rotational displacement along the y and x directions, respectively. In this theory, the shear stress in the thickness direction is a constant value which in fact is not true. On the contrary, in the S-FSDT theory it is assumed that the transverse displacement (w) is divided into the bending component (w_b) and the shear component (w_s) which means that [25]:

$$w = w(bending) + w(shear) \tag{2}$$

Moreover, the rotation variable in the S-FSDT is expressed in terms of the bending components as follows:

$$\varphi = -\frac{\partial w_b}{\partial x}$$
$$\psi = -\frac{\partial w_b}{\partial y} \tag{3}$$

By substituting Eqs. (2, 3) into Eq. (1) the S-FSDT displacement field can be written as follows:

$$\begin{cases} U(x,y,z) = u(x,y) - z\dfrac{\partial w_b}{\partial x} \\ V(x,y,z) = v(x,y) - z\dfrac{\partial w_b}{\partial y} \\ W(x,y,z) = w_b(x,y) + w_s(x,y) \end{cases} \tag{4}$$

In recent years, various size dependent continuum theories such as the couple stress theory, the modified couple stress theory, the strain gradient theory and the nonlocal elasticity theory have proposed. These theories are comprised of information about the inter-atomic forces and internal lengths. Among these theories, the nonlocal elasticity theory of Eringen has been widely applied. But in this theory, unique results cannot be found, because the nonlocal parameter variable has to be used. The classical couple stress theory is one of the higher order continuum theories which contains two additional material length scale parameters along with the classical constants for the elastic material, as elaborated by Mindlin and Tieresten [26], Toupin [27], and Koiter [28]. In fact, the couple stress theory is a special case of Micropolar theory proposed by Cosserat brothers [29]. Recently, a modified couple stress theory, which contains only one additional material length scale parameter in addition to the classical material constants, was proposed by Yang et al. [30]. The modified couple stress theory is more useful than the classical one due to the symmetric couple stress tensor. According to this higher-order continuum theory and using the Hamilton's principle, the governing equations as well as the related boundary conditions along the edges of the rectangular nanoplate can be derived. The equations of the total potential energy (V) are expressed as follows:

$$V = U + \Omega \tag{5}$$

where U is the strain energy and Ω is the work done by external loads. The virtual strain energy can be calculated as follows [31-33]:

$$\delta U = \iiint_V \left(\sigma_{ij}\delta\varepsilon_{ij} + m_{ij}\delta\chi_{ij}\right)dV = 0 \tag{6}$$

where σ_{ij}, ε_{ij}, m_{ij}, χ_{ij} are the stress tensor, the strain tensor, the deviatoric part of the couple stress tensor, and the symmetric curvature tensor, respectively [30-34].

$$\sigma_{ij}=\lambda\varepsilon_{\mathrm{kk}}\delta_{\mathrm{ij}}+2\mu\varepsilon_{ij}\ ;\quad \varepsilon_{ij}=\frac{1}{2}\left(\frac{\partial u_i}{\partial x_j}+\frac{\partial u_j}{\partial x_i}+\frac{\partial u_k}{\partial x_i}\frac{\partial u_k}{\partial x_j}\right) \tag{7}$$

$$m_{ij}=2G_{xy}l^2\chi_{ij} \tag{8}$$

$$\chi_{ij}=\frac{1}{2}\left(\theta_{i,j}+\theta_{j,i}\right)\ ;\ \theta=\frac{1}{2}Curl\left(u\right) \tag{9}$$

where λ and μ are Lame constants, l is a material length scale parameter that is related to the size effect, and θ is the rotatio n vector. The tensors associated in the displacement field in Eqs. (7-9) are as follows:

$$\varepsilon_{xx}=\frac{\partial u}{\partial x}-z\frac{\partial^2 w_b}{\partial x^2}+\frac{1}{2}\left(\frac{\partial w_b}{\partial x}\right)^2+\frac{1}{2}\left(\frac{\partial w_s}{\partial x}\right)^2+\frac{\partial w_b}{\partial x}\frac{\partial w_s}{\partial x} \tag{10a}$$

$$\varepsilon_{yy}=\frac{\partial v}{\partial y}-z\frac{\partial^2 w_b}{\partial y^2}+\frac{1}{2}\left(\frac{\partial w_b}{\partial y}\right)^2+\frac{1}{2}\left(\frac{\partial w_s}{\partial y}\right)^2+\frac{\partial w_b}{\partial y}\frac{\partial w_s}{\partial y} \tag{10b}$$

$$\gamma_{yz}=\frac{\partial w_s}{\partial y} \tag{10c}$$

$$\gamma_{xz}=\frac{\partial w_s}{\partial x} \tag{10d}$$

$$\gamma_{xy}=\left(\frac{\partial u}{\partial y}+\frac{\partial v}{\partial x}\right)-2z\frac{\partial^2 w_b}{\partial x\,\partial y}+\left(\frac{\partial w_b}{\partial x}+\frac{\partial w_s}{\partial x}\right)\left(\frac{\partial w_b}{\partial y}+\frac{\partial w_s}{\partial y}\right) \tag{10e}$$

$$\begin{cases}\chi_x=\frac{1}{2}\left(2\frac{\partial^2 w_b}{\partial x\,\partial y}+\frac{\partial^2 w_s}{\partial x\,\partial y}\right)\\ \chi_y=\frac{1}{2}\left(-2\frac{\partial^2 w_b}{\partial x\,\partial y}-\frac{\partial^2 w_s}{\partial x\,\partial y}\right)\\ \chi_{xy}=\frac{1}{4}\left(-2\frac{\partial^2 w_b}{\partial x^2}+2\frac{\partial^2 w_b}{\partial y^2}-\frac{\partial^2 w_s}{\partial x^2}+\frac{\partial^2 w_s}{\partial y^2}\right)\\ \chi_{xz}=\frac{1}{4}\left(\frac{\partial^2 v}{\partial x^2}-\frac{\partial^2 u}{\partial x\,\partial y}\right)\\ \chi_{yz}=\frac{1}{4}\left(-\frac{\partial^2 u}{\partial y^2}+\frac{\partial^2 v}{\partial x\,\partial y}\right)\end{cases} \tag{11a-e}$$

By using the principle of the minimum potential energy ($\delta V=0$), the nonlinear constitutive equations are derived as:

$$N_{\mathrm{x,x}}+N_{\mathrm{xy,y}}+\tfrac{1}{4}Y_{xz,xy}+\tfrac{1}{4}Y_{yz,yy}=0 \tag{12a}$$

$$N_{\mathrm{xy,x}}+N_{\mathrm{y,y}}-\tfrac{1}{4}Y_{xz,xx}-\tfrac{1}{4}Y_{yz,xy}=0 \tag{12b}$$

$$\begin{aligned}&Q_{\mathrm{x,x}}+Q_{\mathrm{y,y}}+N_{xx}\left(\frac{\partial^2 w_s}{\partial x^2}+\frac{\partial^2 w_b}{\partial x^2}\right)+N_{yy}\left(\frac{\partial^2 w_s}{\partial y^2}+\frac{\partial^2 w_b}{\partial y^2}\right)+2N_{xy}\left(\frac{\partial^2 w_b}{\partial x\,\partial y}+\frac{\partial^2 w_s}{\partial x\,\partial y}\right)-Y_{xx,xy}+\tfrac{1}{2}Y_{yy,xy}\\&+\tfrac{1}{4}Y_{xy,xx}-\tfrac{1}{4}Y_{xy,yy}=0\end{aligned} \tag{12c}$$

$$\begin{aligned}&-M_{\mathrm{x,x}}-2M_{\mathrm{xy,y}}-M_{\mathrm{y,y}}+N_{xx}\left(\frac{\partial^2 w_s}{\partial x^2}+\frac{\partial^2 w_b}{\partial x^2}\right)+N_{yy}\left(\frac{\partial^2 w_s}{\partial y^2}+\frac{\partial^2 w_b}{\partial y^2}\right)+2N_{xy}\left(\frac{\partial^2 w_b}{\partial x\,\partial y}+\frac{\partial^2 w_s}{\partial x\,\partial y}\right)-2Y_{xx,xy}\\&+Y_{yy,xy}+\tfrac{1}{2}Y_{xy,xx}-\tfrac{1}{2}Y_{xy,yy}=0\end{aligned} \tag{12d}$$

In the following equations, *Ni*, *Mi* and *Qi (i= x, y, xy)* and *Yij (i= x, y, xy)* are the stress resultants and non-zero curvature resultants respectively.

$$(N_x,N_y,N_{xy})=\sum_{k=1}^{N}\int_{z_{k-1}}^{z_k}\left(\sigma_x,\sigma_y,\sigma_{xy}\right)dz \tag{13a}$$

$$(M_x, M_y, M_{xy}) = \sum_{k=1}^{N} \int_{z_{k-1}}^{z_k} (\sigma_x, \sigma_y, \sigma_{xy}) z dz \tag{13b}$$

$$(Q_x, Q_y) = \sum_{k=1}^{N} \int_{z_{k-1}}^{z_k} (\sigma_{xz}, \sigma_{yz}) dz \tag{13c}$$

$$\begin{Bmatrix} Y_{xx} \\ Y_{yy} \\ Y_{xy} \\ Y_{xz} \\ Y_{yz} \end{Bmatrix} = \sum_{k=1}^{N} \int_{z_{k-1}}^{z_k} \begin{Bmatrix} m_{xx} \\ m_{yy} \\ m_{xy} \\ m_{xz} \\ m_{yz} \end{Bmatrix} dz \tag{14}$$

In the following equations, the governing equations (Eq. 12) for the rectangular nanoplate can be rewritten as:

$$N_{x,x} + N_{xy,y} + \frac{1}{2} A_s \left(-\frac{\partial^4 u}{\partial x^2 \partial y^2} + \frac{\partial^4 v}{\partial x^3 \partial y} \right) + \frac{1}{2} A_s \left(-\frac{\partial^4 u}{\partial y^4} + \frac{\partial^4 v}{\partial x \partial y^3} \right) = 0 \tag{15a}$$

$$N_{xy,x} + N_{y,y} - \frac{1}{2} A_s \left(-\frac{\partial^4 u}{\partial x^3 \partial y} + \frac{\partial^4 v}{\partial x^4} \right) - \frac{1}{2} A_s \left(-\frac{\partial^4 u}{\partial x \partial y^3} + \frac{\partial^4 v}{\partial x^2 \partial y^2} \right) = 0 \tag{15b}$$

$$\begin{aligned} &Q_{x,x} + Q_{y,y} + N_{xx} \left(\frac{\partial^2 w_b}{\partial x^2} + \frac{\partial^2 w_s}{\partial x^2} \right) + N_{yy} \left(\frac{\partial^2 w_b}{\partial y^2} + \frac{\partial^2 w_s}{\partial y^2} \right) + 2N_{xy} \left(\frac{\partial^2 w_b}{\partial x \partial y} + \frac{\partial^2 w_s}{\partial x \partial y} \right) \\ &-\frac{1}{2} A_s \left(5 \frac{\partial^4 w_b}{\partial x^2 \partial y^2} + 3 \frac{\partial^4 w_s}{\partial x^2 \partial y^2} \right) - \frac{1}{4} A_s \left(\frac{\partial^4 w_b}{\partial x^4} + \frac{1}{2} \frac{\partial^4 w_s}{\partial x^4} + \frac{\partial^4 w_b}{\partial y^4} + \frac{1}{2} \frac{\partial^4 w_s}{\partial y^4} \right) = 0 \end{aligned} \tag{15c}$$

$$\begin{aligned} &-M_{x,x\,x} - 2M_{xy,x\,y} - M_{y,y\,y} + N_{xx} \left(\frac{\partial^2 w_b}{\partial x^2} + \frac{\partial^2 w_s}{\partial x^2} \right) + N_{yy} \left(\frac{\partial^2 w_b}{\partial y^2} + \frac{\partial^2 w_s}{\partial y^2} \right) + 2N_{xy} \left(\frac{\partial^2 w_b}{\partial x \partial y} + \frac{\partial^2 w_s}{\partial x \partial y} \right) \\ &-\frac{5}{2} A_s \left(2 \frac{\partial^4 w_b}{\partial x^2 \partial y^2} + \frac{\partial^4 w_s}{\partial x^2 \partial y^2} \right) - \frac{1}{4} A_s \left(2 \frac{\partial^4 w_b}{\partial x^4} + \frac{\partial^4 w_s}{\partial x^4} + 2 \frac{\partial^4 w_b}{\partial y^4} + \frac{\partial^4 w_s}{\partial y^4} \right) = 0 \end{aligned} \tag{15d}$$

The axial and flexural rigidities of orthotropic and isotropic nanoplates are given by:

$$\begin{aligned} &\left[A_{ij} \right] = \sum_{k=1}^{N} \left[\overline{Q}_{ij} \right]_k (h_k - h_{k-1}) = \sum_{k=1}^{N} \left[\overline{Q}_{ij} \right]_k t_k \ , \ N: Number\ of\ layers \\ &\left[B_{ij} \right] = \frac{1}{2} \sum_{k=1}^{N} \left[\overline{Q}_{ij} \right]_k (h_k^2 - h_{k-1}^2) = \sum_{k=1}^{N} \left[\overline{Q}_{ij} \right]_k t_k \overline{z}_k \\ &\left[D_{ij} \right] = \frac{1}{3} \sum_{k=1}^{N} \left[\overline{Q}_{ij} \right]_k (h_k^3 - h_{k-1}^3) = \sum_{k=1}^{N} \left[\overline{Q}_{ij} \right]_k \left(t_k \overline{z}_k^2 + \frac{t_k^3}{12} \right) \\ &Q_{11} = \frac{E_x}{1 - \upsilon_{xy} \upsilon_{yx}}, \ Q_{22} = \frac{E_y}{1 - \upsilon_{xy} \upsilon_{yx}}, \ Q_{12} = \frac{\upsilon_{yx} E_x}{1 - \upsilon_{xy} \upsilon_{yx}}, \ Q_{66} = G_{xy} \\ &Q_{11} = \frac{E}{1 - \upsilon^2} = Q_{22}, \ Q_{12} = \frac{\upsilon E}{1 - \upsilon^2}, \ Q_{66} = G \\ &\left[H_{44} \right]_k = \left[H_{55} \right]_k = \sum_{k=1}^{N} \int_{z_{k-1}}^{z_k} G dz \ , \ A_s = \sum_{k=1}^{N} \int_{z_{k-1}}^{z_k} G l^2 dz \ , \ C_{44} = C_{55} = G \end{aligned} \tag{16}$$

In Eq. (16), A_{ij}, B_{ij} and D_{ij} are the extensional stiffness, the bending stiffness and the extension-bending coupling matrix, respectively. Moreover, E_x, E_y and E are the Young's elasticity modules, v_{xy}, v_{yx} and v are the Poisson's ratio and G_{xy}, G_{xz} and G_{yz} and G are the shear modules for orthotropic and isotropic materials, respectively. The stress resultants in Eq. (13) in the displacement field by using Eq.16 are defined as:

$$\begin{bmatrix} N_{xx} \\ N_{yy} \\ N_{xy} \\ M_{xx} \\ M_{yy} \\ M_{xy} \\ Q_{y} \\ Q_{x} \end{bmatrix} = \begin{bmatrix} A_{11} & A_{12} & 0 & 0 & 0 & 0 & 0 & 0 \\ A_{12} & A_{22} & 0 & 0 & 0 & 0 & 0 & 0 \\ 0 & 0 & A_{66} & 0 & 0 & 0 & 0 & 0 \\ 0 & 0 & 0 & D_{11} & D_{12} & 0 & 0 & 0 \\ 0 & 0 & 0 & D_{12} & D_{22} & 0 & 0 & 0 \\ 0 & 0 & 0 & 0 & 0 & D_{66} & 0 & 0 \\ 0 & 0 & 0 & 0 & 0 & 0 & H_{44} & 0 \\ 0 & 0 & 0 & 0 & 0 & 0 & 0 & H_{55} \end{bmatrix} \times \begin{bmatrix} \frac{\partial u}{\partial x}+\frac{1}{2}\left(\frac{\partial w_b}{\partial x}\right)^2+\frac{1}{2}\left(\frac{\partial w_s}{\partial x}\right)^2+\frac{\partial w_b}{\partial x}\frac{\partial w_s}{\partial x} \\ \frac{\partial v}{\partial y}+\frac{1}{2}\left(\frac{\partial w_b}{\partial y}\right)^2+\frac{1}{2}\left(\frac{\partial w_s}{\partial y}\right)^2+\frac{\partial w_b}{\partial y}\frac{\partial w_s}{\partial y} \\ \frac{\partial u}{\partial y}+\frac{\partial v}{\partial x}+\left(\frac{\partial w_b}{\partial x}+\frac{\partial w_s}{\partial x}\right)\left(\frac{\partial w_b}{\partial y}+\frac{\partial w_s}{\partial y}\right) \\ -\frac{\partial^2 w_b}{\partial x^2} \\ -\frac{\partial^2 w_b}{\partial y^2} \\ -\frac{\partial^2 w_b}{\partial x\,\partial y} \\ \frac{\partial w_s}{\partial y} \\ \frac{\partial w_s}{\partial x} \end{bmatrix} \tag{17}$$

The nonuniform in-plane forces in pre-buckling conditions are as follows. Parabolically varying in-plane load [35]:

$$\begin{cases} N_{xx} = -4k_1 N^0 \dfrac{y}{L_y}\left(1-\dfrac{y}{L_y}\right) \\ N_{yy} = -4k_2 N^0 \dfrac{x}{L_x}\left(1-\dfrac{x}{L_x}\right) \end{cases} \tag{18}$$

Sinusoidal varying in-plane load [36]:

$$\begin{cases} N_{xx} = -k_1 \dfrac{\pi}{2} N^0 \operatorname{Sin}\left(\dfrac{\pi y}{L_y}\right) \\ N_{yy} = -k_2 \dfrac{\pi}{2} N^0 \operatorname{Sin}\left(\dfrac{\pi x}{L_x}\right) \end{cases} \tag{19}$$

Linearly varying in-plane load [36-37]:

$$\begin{cases} N_{xx} = -k_1 N^0 \left(1-\eta \dfrac{y}{L_y}\right) \\ N_{yy} = -k_2 N^0 \left(1-\eta \dfrac{x}{L_x}\right) \end{cases} \tag{20}$$

As afore-mentioned about the linear load, $\eta=0$ (Uniform load), $\eta=1$ (Triangular load). Moreover, N^0 is the critical in-plane load in buckling conditions. By substituting Eqs. (17) and (18-20) in Eq. (15), and also by considering the pre-buckling condition, the stability equations in the form of displacement components based on S-FSDT and including couple stress effect are expressed as follows:

$$\begin{aligned} & H_{44}\frac{\partial^2 w_s}{\partial x^2}+H_{55}\frac{\partial^2 w_s}{\partial y^2}+k_1 N_{xx}\left(\frac{\partial^2 w_b}{\partial x^2}+\frac{\partial^2 w_s}{\partial x^2}\right)+k_2 N_{yy}\left(\frac{\partial^2 w_b}{\partial y^2}+\frac{\partial^2 w_s}{\partial y^2}\right) \\ & -A_s\left[\frac{1}{2}\left(5\frac{\partial^4 w_b}{\partial x^2\partial y^2}+3\frac{\partial^4 w_s}{\partial x^2\partial y^2}\right)-\frac{1}{4}\left(\frac{\partial^4 w_b}{\partial x^4}+\frac{1}{2}\frac{\partial^4 w_s}{\partial x^4}+\frac{\partial^4 w_b}{\partial y^4}+\frac{1}{2}\frac{\partial^4 w_s}{\partial y^4}\right)\right]=0 \\ & D_{11}\frac{\partial^4 w_b}{\partial x^4}+\left(2D_{12}+2D_{66}\right)\frac{\partial^4 w_b}{\partial x^2\partial y^2}+D_{22}\frac{\partial^4 w_b}{\partial y^4}+k_1 N_{xx}\left(\frac{\partial^2 w_b}{\partial x^2}+\frac{\partial^2 w_s}{\partial x^2}\right)+k_2 N_{yy}\left(\frac{\partial^2 w_b}{\partial y^2}+\frac{\partial^2 w_s}{\partial y^2}\right) \\ & -A_s\left[\frac{5}{2}\left(2\frac{\partial^4 w_b}{\partial x^2\partial y^2}+\frac{\partial^4 w_s}{\partial x^2\partial y^2}\right)-\frac{1}{4}\left(2\frac{\partial^4 w_b}{\partial x^4}+\frac{\partial^4 w_s}{\partial x^4}+2\frac{\partial^4 w_b}{\partial y^4}+\frac{\partial^4 w_s}{\partial y^4}\right)\right]=0 \end{aligned} \tag{21a-b}$$

3. Exact solution procedure

In this study, different analytical boundary conditions are applied to solve the obtained stability equations which can be written in an explicit mathematically form as [32-33]:

$$\text{Free edge (F):}\quad X_i=\left[\sin^2(\alpha_i x_i)+1\right]\cos^2(\alpha_i x_i)\ ;\ i=1,2 \tag{22a}$$

$$\text{Clamped (C):}\quad X_i=\sin^2(\alpha_i x_i)\ ;\ i=1,2 \tag{22b}$$

$$\text{Simply supported (S):}\quad X_i=\sin(\alpha_i x_i)\ ;\ i=1,2 \tag{22c}$$

Where m and n are the half wave numbers, $\alpha_1=m\pi/L_x$, $\alpha_2=n\pi/L_y$, $x_1=x$, and $x_2=y$ or terms used in the x and y direction to represents the displacement functions. The displacement function is used in the following form:

$$w_k(x,y)=W_k X_i X_j\ ;\ k=s,b;\ i=1,2\ ;\ j=1,2 \tag{23}$$

By substituting the expression of w_k in Eq. (21), the explicit relation for buckling loads with various boundary conditions can be obtained. The stability equations and closed-form boundary conditions yield a set of following algebraic equations:

$$\begin{Bmatrix} Eq.20a \\ Eq.20b \end{Bmatrix}=\begin{bmatrix} k_{11} & k_{12} \\ k_{21} & k_{22} \end{bmatrix}\begin{Bmatrix} W_b \\ W_s \end{Bmatrix} \tag{24}$$

where *kij (i, j=1, 2)* are the coefficients of constants terms. To obtain the critical load the following equation is employed:

$$q=\left[Eq.21a \quad Eq.21b\right],\ u=\left[W_b \quad W_s\right] \tag{25}$$

$$J=jacobian(q,u)\rightarrow \det[J]=0 \tag{26}$$

4. Results and Discussion

The validation and comparison of the obtained results with other research results should obviously be carried out before investigating various parameters of this study. Therefore, Fig. 2 is presented to compare and validate these formulation results with those of other articles. As shown in Fig. 2, the results are obtained in two ways by means of the analytical solution. However, in order to compare results in Tables 1 and 2, the results of [19] and [38] studies are employed while they are obtained using the first order shear deformation theory, the differential quadrature method (DQM), as well as the Eringen nonlocal elasticity theory. The result of [39] study is added for further confirmation due to the minor errors in the numerical solutions while its results are obtained through the molecular dynamics solution. Therefore, observing only Fig. 2 does not enable us to ascertain the fact that the present results are validated due to the difference between the results in both cases. However, by examining Tables 1 and 2, one can strongly express that the modified first order shear deformation theory (S-FSDT) results appropriately correspond to the molecular dynamic results. Since this solution is an exact one, the proximity of the results clearly confirms this premise that accurate and appropriate results are obtained by combining the modified first order shear deformation theory and the exact solution of the results. Comparing Fig. 2 with the results shown in Tables 1 and 2 confirms that the removal of the shear stress correction factors in moderately thick plates affects the critical load results. Because, the generated difference in the contractual FSDT by employing this factor when compared with the accurate results is removed in the S-FSDT. According to Tables 1, 2 and Fig. 2, the thinner we assume the plate, the closer the results become to the FSDT results and the numerical solution, while their accuracy decreases; because, FSDT is not applicable to analyze thin plates and the classical plate theory (CPT) is more applicable in this case.

E=1TPa, υ=0.3, h=0.34 nm, μ=1.81nm², β=Lx/Ly=1, k1=1, k2=1, k_s=5/6, SSSS [19, 38-39]

E=1TPa, υ=0.3, h=0.34 nm, β=1, k1=1, k2=1, l=2.91nm, η=0, SSSS [Present]

Figs. 3a and 3b are presented to show the impact of uniaxial and biaxial loadings. The sandwich panel is determined as square and rectangular in the first and second figure, respectively. This investigation is carried out under monotonic and linear loadings due to the changes in *m* and *n* parameters. In the first figure, the critical load results obtained from *k1=0*, *k2=1* fully corresponds to the results of *k1=1*, *k2=0*; whereas, by investigating the second figure and rectangular plates, it is observed that the results obtained from *k1=0*, *k2=1* show higher values. Moreover, it is observed that the critical load increases with an increase in m and n values.

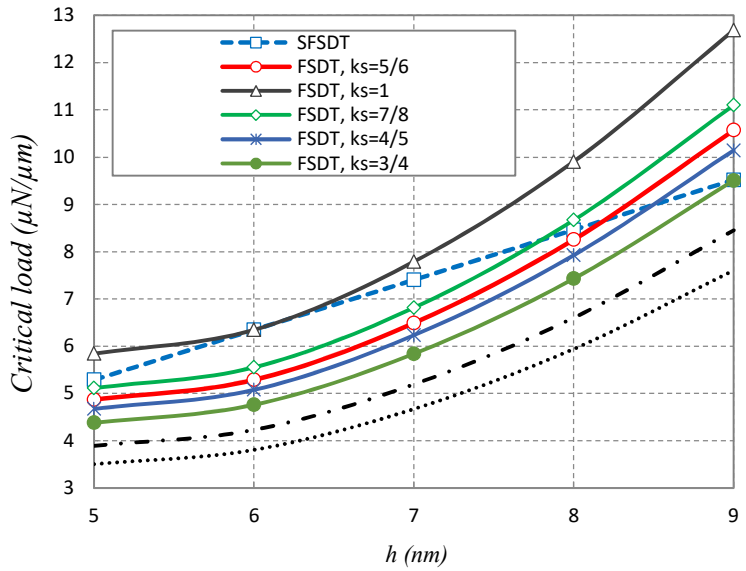

Fig. 2. Comparison of S-FSDT with FSDT in local conditions for the sandwich plate *(Lx=15h, η=1, k1=k2=1, SSSS, Al)*

Table 1. Comparison of results for the critical biaxial buckling load for the single-layered graphene sheet and all edges simply supported obtained from DQ method [19, 38], and the molecular dynamics simulation [39].

Critical buckling load (*Pa.m*)				
Present study	FSDT-DQM [19]	FSDT-DQM [38]	MD results [39]	Lx=Ly (*nm*)
1.0835	1.0749	1.0809	1.0837	4.99
0.6538	0.6523	0.6519	0.6536	8.080
0.4330	0.4356	0.4350	0.4331	10.77
0.2615	0.2645	0.2639	0.2609	14.65
0.1720	0.1751	0.1748	0.1714	18.51
0.1198	0.1239	0.1237	0.1191	22.35
0.0896	0.0917	0.0914	0.0889	26.22
0.0696	0.0707	0.0705	0.0691	30.04
0.0559	0.0561	0.0560	0.0554	33.85
0.0454	0.0453	0.0451	0.0449	37.81

Table 2. Comparison of the present results with those of DQ method [38] and the molecular dynamics (MD) simulation [39] for different aspect ratios of orthotropic single-layered graphene sheets under the uniform biaxial compression.

Critical buckling load (*Pa.m*)			
FSDT-DQM [38]	MD results [39]	S-FSDT, Exact Present study	*Lx/Ly*
0.5115	0.5101	0.5105	0.5
0.5715	0.5693	0.5698	0.75
0.6622	0.6595	0.6599	1.25
0.7773	0.7741	0.7747	1.5
1.0222	1.0183	1.0180	1.75
1.1349	1.1297	1.1301	2

Table 3. Mechanical properties of the sandwich plate

Section	Material	Elasticity parameters
Faces	Graphene sheet [23]	*Ex=1765Gpa, Ey=1588Gpa, v_{xy}=0.3, v_{yx}=Ey×v_{xy}/Ex*
Core	Epoxy resin	*E=2.8Gpa, v=0.35*
	Aluminum alloy	*E=70Gpa, v=0.33*

In Fig. 4a, the changes of the length scale parameter against the changes in t_1 to t_2 thickness ratio are investigated while t_2 is alterable. As can be seen, the critical load increases with an increase in l parameter. This parameter will increase more when T value becomes smaller and core to face thickness ratio increases as well. In fact, one can conclude according to this figure that the impact of the length scale parameter on the critical load resulted from various thickness is not significant. However, these results are different in Fig. 4b.

Fig. 4b is presented according to different boundary conditions. As can be seen, the critical load results at a variety of boundary conditions increases with an increased l parameter as compared with the case in which this impact is disregarded ($l=0$). According to Fig. 4b, the highest critical load is obtained at the CFCF boundary condition and the lowest one is obtained at the SFSF boundary condition. In conclusion, the impact of the length scale parameter on the boundary condition is much higher than its impact on other parameters. According to Fig. 4b, a thicker core exhibits higher impact force.

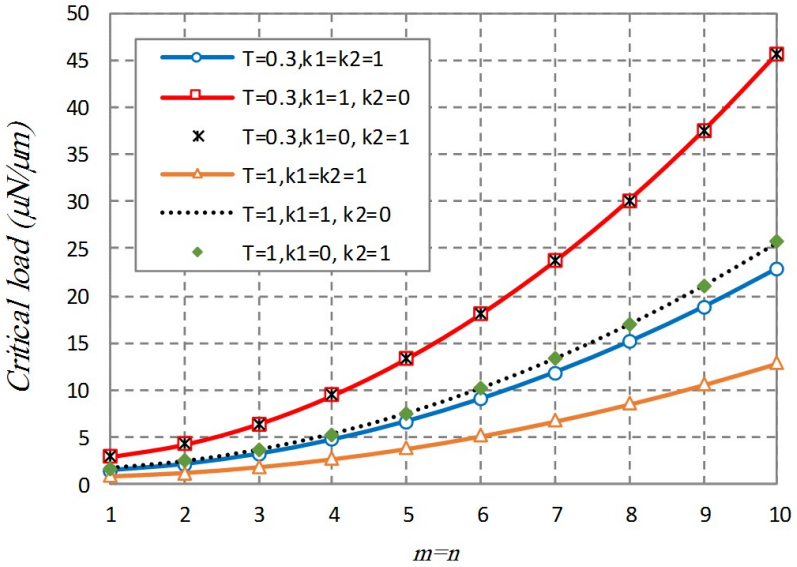

Fig. 3a. The effect of the load direction versus wave numbers on two thickness for the core *(β=Lx/Ly=1, l=2h, Lx=15h, SSSS, Epoxy, η=0)*

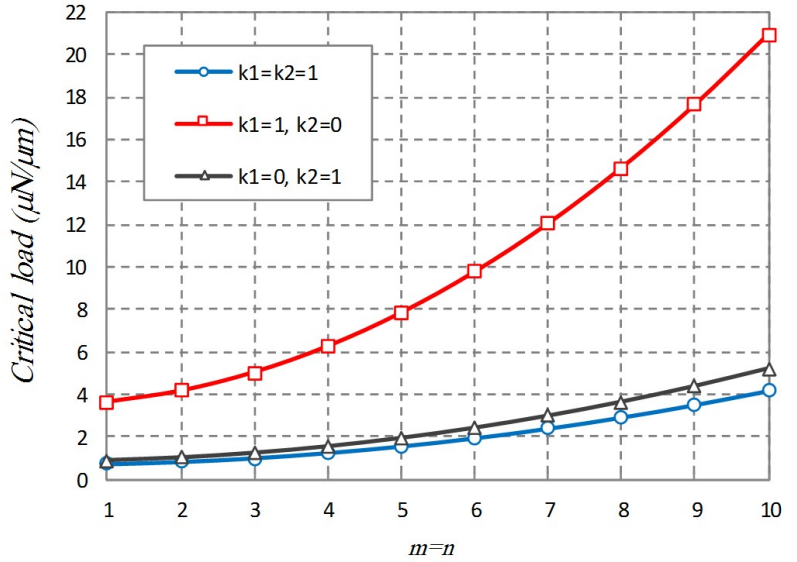

Fig. 3b. The effect of the load direction versus wave numbers on the rectangular plate *(β=2, T=1, l=2h, Lx=15h, SSSS, Epoxy, η=0)*

Fig. 5 indicates changes in the sandwich panel by using two core materials. This is obvious that a stronger core increases the critical load. However, investigating the graph indicates that with $h>0.08\mu m$ thickness, the graph line shows a steep upward trend. This increasing level occurs in the graph of both cores but $Lx=20h$. In fact, the increase in the length and the width of high thickness plates provides higher critical loads.

In order to determine the impact of the length scale parameter (l) on buckling results, Fig. 6 is provided. To this aim, two boundary conditions of CCCC and SSSS with two loading modes are investigated. As the results indicate, the critical load value at CCCC boundary condition is higher than SSSS value. When we disregard the impact of the length scale, the impact of the loading and the boundary condition type is insignificant at larger T values, but the increased length parameter results in higher difference between any loading type results at two boundary conditions. This can be inferred from the difference between the results of CCCC that $\eta=0$ and SSSS, $\eta=0.5$ at $l^*>7$.

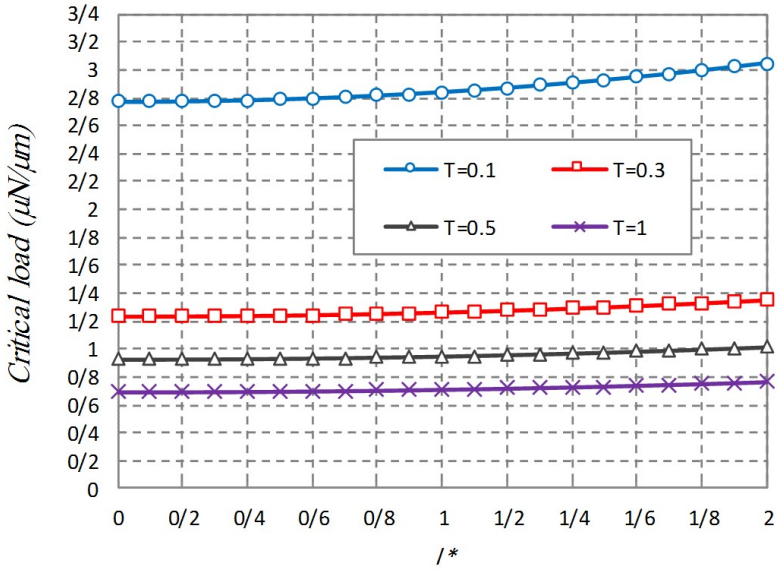

Fig. 4a. The length scale parameter versus the thickness (β=1, T=t1/t2, Lx=20h, η=0, k1=k2=1, l^*=l/h, m=n=1, SSSS, Epoxy)

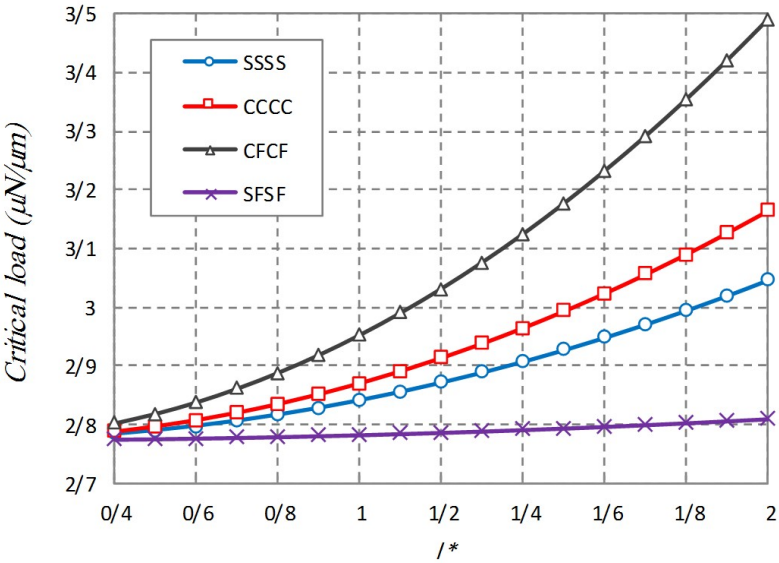

Fig. 4b. Length scale parameter versus boundary conditions (β=1, T=0.1, Lx=20h, η=0, k1=k2=1, l^*=l/h, m=n=1, Epoxy)

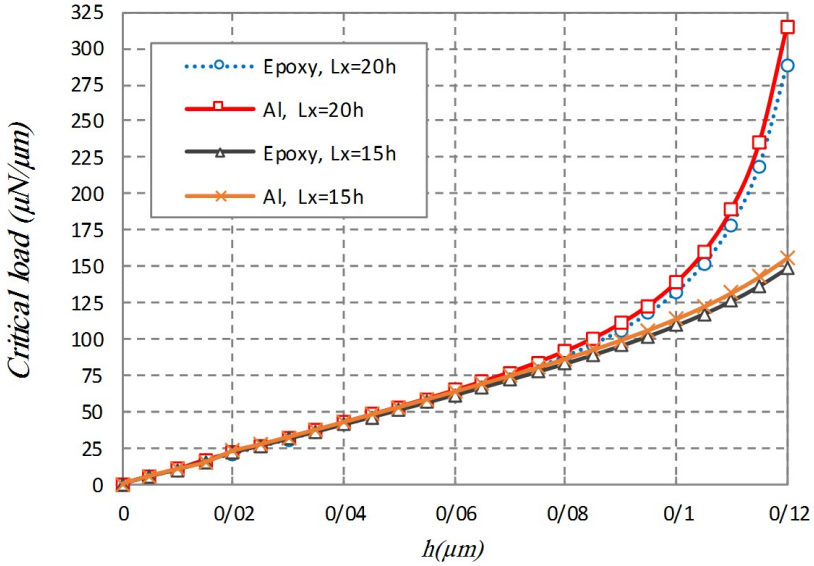

Fig. 5. Variation of the panel thickness versus various core materials (β=1, η=1, Lx=15h, k1=k2=1, l=0.5h, m=n=1, CFCF)

In Fig. 7, the changes in the ratio of the face thickness to the core are investigated when the core thickness is assumed as variable against two boundary conditions. The results are obtained where the core is made of aluminum alloy and sandwich

panel has a lower thickness (Lx=20h). As the Figure indicates, the critical load decreases when core thickness value approaches to the face thickness value; moreover, the difference in the results is insignificant at two boundary conditions of SSSS and SFSF. In fact, the impact of the core thickness on the boundary condition is obvious. Therefore, the impact of the core thickness in critical load results is higher than those of the loading type as well as the boundary condition.

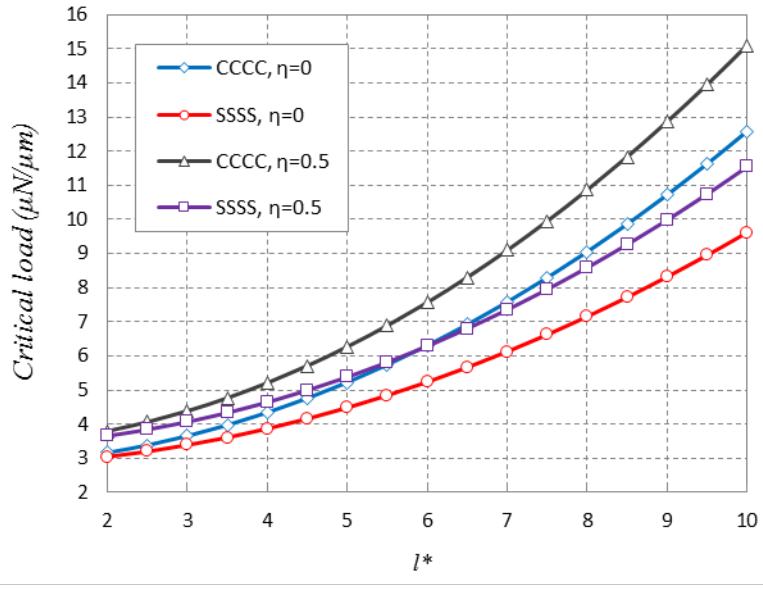

Fig. 6. Variation of the length scale parameter versus the loading type on the critical load in various boundary conditions (*β=1, Lx=20h, k1=k2=1, T=0.1, l*=l/h, m=n=1, Epoxy*)

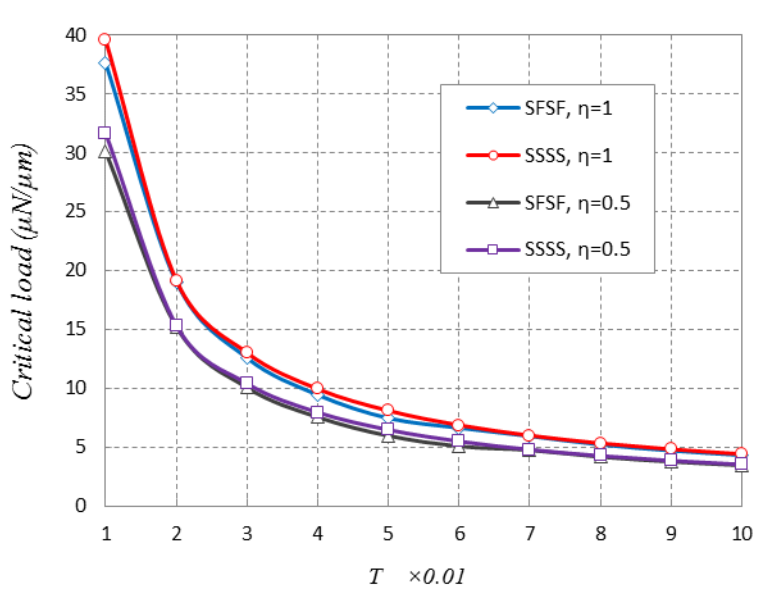

Fig. 7. The effect of the loading type on the critical load in various boundary conditions (*β=1, Lx=20h, k1=k2=1, l=h, m=n=1, Al*)

The impact of loading types on the sandwich panel with the thickness change of the panel at two boundary conditions of CFCF and SSSS are investigated in figure 8a and 8b, respectively. To this aim, the Epoxy for the core in the first Figure and the aluminum alloy in the second figure are used; however, the thicker panel is used in the second figure. As can be seen, at CFCF boundary condition, critical load changes are more irregular compared with those of SSSS boundary condition. In fact, at CFCF boundary condition within the range of 10<h<20 nm, the highest irregularity is observed in the graph. The direct effect of thickness on the length scale parameter in the formulation of the modified couple stress theory is observed. As a matter of fact, as it is known, when returning to the Eringen nonlocal theory in which the small scale is directly related to the length of the plate, the couple stress theory is dependent on the thickness of the plate. The second reason is the unforeseen behavior of free edges after deformation which leads to the irregular curve. In fact, this boundary condition includes erratic outcomes.

Given the loading type, this is clear that in the case of a linear and nonuniform triangular loading, the highest critical load will be obtained. In addition, when loading is considered as a hyperbolic function, the critical load has the lowest value. In fact, in linear loading, as the in-plane load gets farther from the plate center, the critical load will increase. A possible reason can be

the combination of the in-plane torsion to the in-plane pressure. Consequently, the pressure decreases as the load center distances from the plate center in x and y directions and it is substituted by the in-plane torsion while the plate buckles as it twists. Clearly, a higher in-plane torsional force is needed to move the plate into the bucking region.

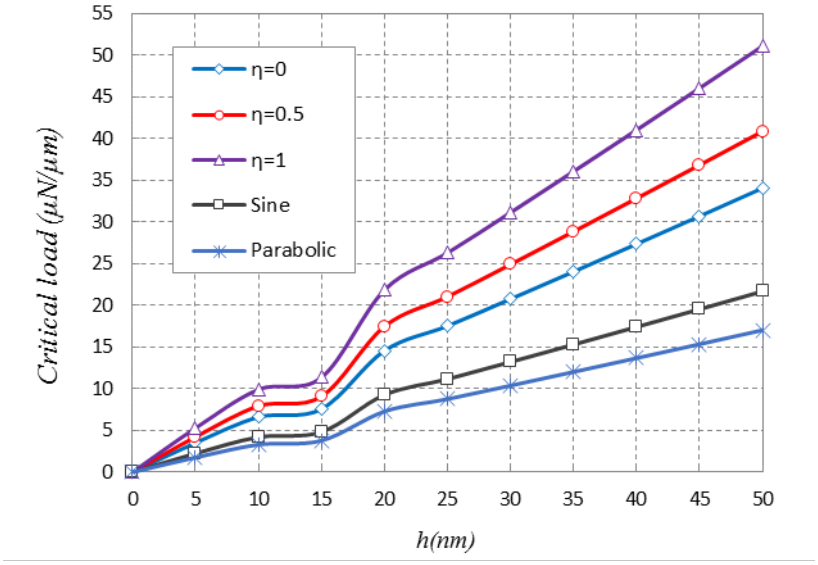

Fig. 8a. The effect of various loading versus panel thickness on critical load (*β=1, Lx=15h, k1=k2=1, l=0.5h, m=n=1, CFCF, Epoxy*)

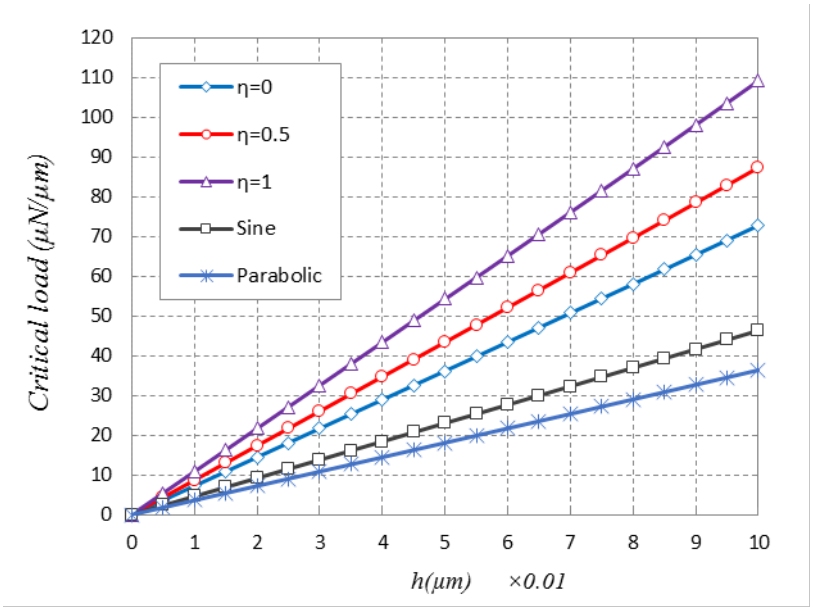

Fig. 8b. The effect of various loadings versus the panel thickness on the critical load (*β=1, Lx=10h, k1=k2=1, l=0.5h, m=n=1, SSSS, Al*)

The thickness change of t_2 against the change in β parameter is shown in Fig. 9. To this aim, the boundary condition of CFCF and the Epoxy for the core are applied. As can be seen, the increase in β results in decreased critical load. The critical load amount decreases more slowly from β =5 onward, and the highest slope of graph is as $1<\beta<3$ in which the critical load slope is very steep.

In order to investigate the impact of increasing the thickness, layers of the sandwich panel of Fig. 10 are investigated. The graph indicates that the impact of an increase in the core thickness is higher than that of the faces thickness. As the core gets thicker, the impact will be higher than the factor t2/t1=1.5. In fact, according to the Figure, the impact of the core thickness on increasing the plate's resistance against in-plane loads is higher than that of the face when the face materials have a higher strength. The reason probably is that, by increasing the core thickness, faces will have a greater distance from the plate center in z direction, and their moment resistance increases the strength of the sandwich plate.

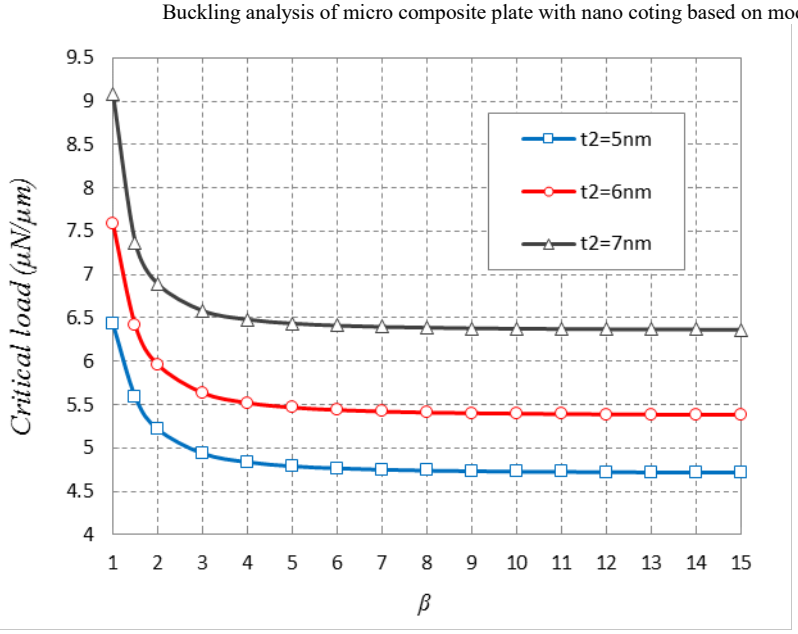

Fig. 9. Variation of the aspect ratio versus the core thickness on the critical load (*Ly=15h, l=h, η=1, k1=k2=1, CFCF, Epoxy*)

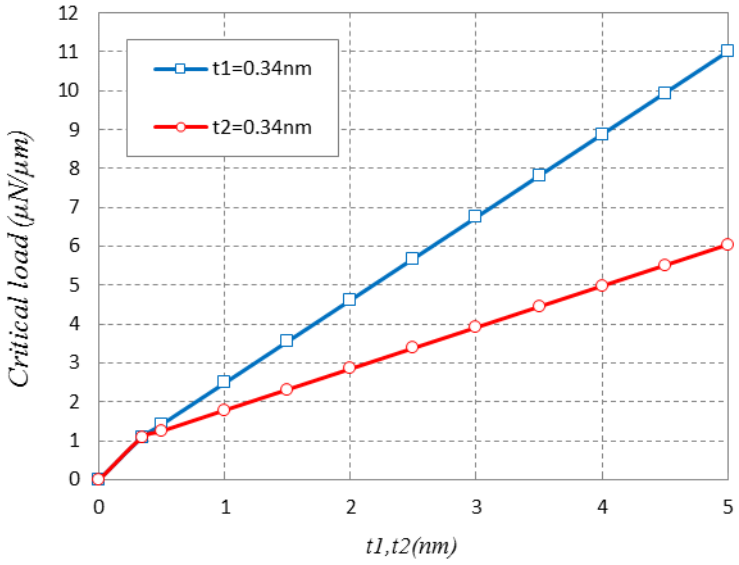

Fig. 10. Variation of the core thickness versus the face thickness (*l=h, Lx=15h, η=1, k1=k2=1, SSSS, Epoxy*)

5. Conclusion

This study investigated the buckling of micro/nano graphene-coated sandwich panels. For this purpose, the simplified first order shear deformation theory was employed to obtain the governing equations by taking into account the Von-Karman nonlinear strains. The impact of the small scale was investigated by using the modified couple stress theory. Moreover, the exact solution was used to extract the results by changing various parameters. In conclusion, some of the important results achieved from the present study are as follows:

- The maximum critical load value is at the CFCF boundary condition and the minimum is at the SFSF boundary condition.
- The impact of the core thickness increase on increasing the value of the critical load is higher if the face has higher strength even if the core is soft and with a low strength. It means that if the face material is strong, it increases the plate strength against in-plane loads and a stronger core is not required.

References

[1] Ovid'ko, I.A., Mechanical properties of graphene, *Review on Advanced Materials Science*, 34, 2013, pp. 1-11.
[2] Walker, L.S., Marotto, V.R., Rafiee, M.A., Koretkar, N., Corral, E.L., Toughening in graphene ceramic composites, *ACS Nano*, 5, 2011, pp. 3182-90.
[3] Kvetkova, L., Duszova, A., Hvizdos, P., Dusza, J., Kun, P., Balazsi, C., Fracture toughness and toughening mechanisms in graphene platelet reinforced Si 3 N 4 composites, *Scripta Materialia*, 66, 2012, pp. 793-796.

[4] Liang, J., Huang, Y., Zhang, L., Wang, Y., Ma, Y., Guo, T., Chen, Y., Molecular-level dispersion of graphene into poly (vinyl alcohol) and effective reinforcement of their nanocomposites, *Advanced Functional Materials*, 19, 2009, pp. 2297-2302.
[5] Rafiee, M.A., Rafiee, J., Srivastana, I., Wang, Z., Song, H., Yu, Z-Z., Koratkar, N., Fracture and fatigue in graphene Nano composites, *Small*, 6, 2010, pp. 179-83.
[6] Plantema, F.J., *Sandwich Construction: The Bending and Buckling of Sandwich Beams, Plates, and Shells*, Jon Wiley and Sons, New York, 1966.
[7] Kraus, G., Interactions of Elastomers and Reinforcing Fillers, *Rubber Chemistry and Technology*, 38, 1965, pp. 1070-1114.
[8] Malekzadeh, P., Setoodeh, A.R., Beni, A.A., Small scale effect on the thermal buckling of orthotropic arbitrary straight-sided quadrilateral nanoplates embedded in an elastic medium, *Composite Structures*, 93, 2011, pp. 2083–2089.
[9] Zenkour, A.M., Sobhy, M., Nonlocal elasticity theory for thermal buckling of nanoplates lying on Winkler–Pasternak elastic substrate medium, *Physica E*, 53, 2013, pp. 251–259.
[10] Murmu, T., Sienz, J., Adhikari, S., Arnold, C., Nonlocal buckling of double-nanoplate-systems under biaxial compression, *Composites: Part B*, 44, 2013, pp. 84–94.
[11] Wang, Y-Z., Cui, H-T., Li, F-M., Kishimoto, K., Thermal buckling of a nanoplate with small-scale effects, *Acta Mechanica*, 224, 2013, pp. 1299–1307.
[12] Malekzadeh, P., Alibeygi, A., Thermal Buckling Analysis of Orthotropic Nanoplates on Nonlinear Elastic Foundation, *Encyclopedia of Thermal Stresses*, 2014, pp. 4862-4872.
[13] Mohammadi, M., Farajpour, A., Moradi, A., Ghayour, M., Shear buckling of orthotropic rectangular graphene sheet embedded in an elastic medium in thermal environment, *Composites: Part B*, 56, 2014, pp. 629–637.
[14] Radic, N., Jeremic, D., Trifkovic, S., Milutinovic, M., Buckling analysis of double-orthotropic nanoplates embedded in Pasternak elastic medium using nonlocal elasticity theory, *Composites: Part B*, 61, 2014, pp. 162–171.
[15] Karlicic, D., Adhikari, S., Murmu, T., Exact closed-form solution for non-local vibration and biaxial buckling of bonded multi-nanoplate system, *Composites: Part B*, 66, 2014, pp. 328-339.
[16] Anjomshoa, A., Shahidi, A.R., Hassani, B., Jomehzadeh, E., Finite Element Buckling Analysis of Multi-Layered Graphene Sheets on Elastic Substrate Based on Nonlocal Elasticity Theory, *Applied Mathematical Modelling*, 38, 2014, pp. 1-22.
[17] Radebe, I.S., Adali, S., Buckling and sensitivity analysis of nonlocal orthotropic nanoplates with uncertain material properties, *Composites: Part B*, 56, 2014, pp. 840–846.
[18] Nguyen, T.K., Vo, T. P., Nguyen, B.D., Lee, J., An analytical solution for buckling and vibration analysis of functionally graded sandwich beams using a quasi-3D shear deformation theory, *Composite Structures*, 156, 2015, pp. 238-252.
[19] Golmakani, M.E., Rezatalab, J., Non uniform biaxial buckling of orthotropic Nano plates embedded in an elastic medium based on nonlocal Mindlin plate theory, *Composite Structures*, 119, 2015, pp. 238-250.
[20] Jamali, M., Shojaee, T., Mohammadi, B., Uniaxial buckling analysis comparison of nanoplate and nanocomposite plate with central square cut out using domain decomposition method, *Journal of Applied and Computational Mechanics*, 2, 2016, pp. 230-242.
[21] Radic, N., Jeremić, D., Thermal buckling of double-layered graphene sheets embedded in an elastic medium with various boundary conditions using a nonlocal new first-order shear deformation theory, *Composites: Part B*, 97, 2016, pp. 201-215.
[22] Zarei, M. Sh., Hajmohammad, M. H., Nouri, A., Dynamic buckling of embedded laminated nanocomposite plates based on sinusoidal shear deformation theory, *Journal of Applied and Computational Mechanics*, 2, 2016, pp. 254-261.
[23] Malikan, M., Jabbarzadeh, M., Dastjerdi, Sh., Non-linear Static stability of bi-layer carbon nanosheets resting on an elastic matrix under various types of in-plane shearing loads in thermo-elasticity using nonlocal continuum, *Microsystem Technologies*, 23(7), 2017, pp. 2973-2991.
[24] Mindlin, R.D., Influence of Rotatory Inertia and Shear on Flexural Motions of Isotropic, Elastic Plates, *Journal of Applied Mechanics*, 73, 1951, pp. 31–38.
[25] Thai, H-T., Choi, D-H., A simple first-order shear deformation theory for laminated composite plates, *Composite Structures*, 106, 2013, pp. 754-763.
[26] Mindlin, R.D., Tiersten, H.F., Effects of couple-stresses in linear elasticity, *Archive for Rational Mechanics and Analysis*, 11, 1962, pp. 415–48.
[27] Toupin, R.A., Elastic materials with couple stresses, *Archive for Rational Mechanics and Analysis*, 11, 1962, pp. 385-414.
[28] Koiter, W. T., Couple stresses in the theory of elasticity, *I and II. Proc K Ned Akad Wet (B)*, 67, 1964, pp. 17-44.
[29] Cosserat, E., Cosserat, F., Theory of deformable bodies, *Scientific Library, 6. Paris: A. Herman and Sons, Sorbonne*, 6, 1909.
[30] Yang, F., Chong, A.C.M., Lam, D.C.C., Tong, P., Couple stress based strain gradient theory for elasticity, *International Journal of Solids and Structures*, 39, 2002, pp. 2731–43.
[31] Akgöz, B., Civalek, O., Free vibration analysis for single-layered graphene sheets in an elastic matrix via modified couple stress theory, *Materials and Design*, 42, 2012, pp. 164–171.
[32] Malikan, M., Electro-mechanical shear buckling of piezoelectric nanoplate using modified couple stress theory based on simplified first order shear deformation theory, *Applied Mathematical Modeling*, 48, 2017, pp. 196–207.
[33] Malikan, M., Analytical prediction for buckling of nanoplate subjected to nonuniform compression based on four-variable plate theory, *Journal of Applied and Computational Mechanics*, 3(3), 2017, pp. 218-228.
[34] Thai, H-T., Thuc, P. Vo, Nguyen, T-K., Lee, J., Size-dependent behavior of functionally graded sandwich microbeams based on the modified couple stress theory, *Composite Structures*, 123, 2015, pp. 337–349.
[35] Dey, T., Ramachandra, L.S., Buckling and postbuckling response of sandwich panels under non-uniform mechanical edge loadings, *Composites: Part B*, 60, 2014, pp. 537–545.

[36] Leissa, A.W., Kang, Jae-Hoon, Exact solutions for vibration and buckling of an SS-C-SS-C rectangular plate loaded by linearly varying in-plane stresses, *International Journal of Mechanical Sciences*, 44, 2002, pp. 1925–1945.
[37] Hwang, I., Seh Lee, J., Buckling of Orthotropic Plates under Various Inplane Loads, *KSCE Journal of Civil Engineering*, 10, 2006, pp. 349–356.
[38] Golmakani, M.E., Sadraee Far, M.N., Buckling analysis of biaxially compressed double-layered graphene sheets with various boundary conditions based on nonlocal elasticity theory, *Microsystem Technologies*, 23, 2017, pp. 2145-2161.
[39] Ansari, R., Sahmani, S., Prediction of biaxial buckling behavior of single-layered graphene sheets based on nonlocal plate models and molecular dynamics simulations, *Applied Mathematical Modeling*, 37, 2013, pp. 7338–7351.